

# Multi-microjoule GaSe-based mid-infrared optical parametric amplifier with an ultra-broad idler spectrum covering 4.2-16 $\mu\text{m}$

KUN LIU<sup>1,2</sup>, HOUKUN LIANG<sup>1,\*</sup>, LIFENG WANG<sup>1</sup>, SHIZHEN QU<sup>1,2</sup>, HAO LI<sup>1</sup>, QI JIE WANG<sup>2,\*</sup>, YING ZHANG<sup>1</sup>

*1 Precision Measurements Group, Singapore Institute of Manufacturing Technology, 2 Fusionopolis Way, 138634, Singapore*

*2 School of Electrical & Electronic Engineering & The Photonics Institute, Nanyang Technological University 639798, Singapore*

*\*Corresponding author: hkliang@simtech.a-star.edu.sg, qjwang@ntu.edu.sg*

Received XX Month XXXX; revised XX Month, XXXX; accepted XX Month XXXX; posted XX Month XXXX (Doc. ID XXXXX); published XX Month XXXX

**We report a multi-microjoule, ultra-broadband mid-infrared optical parametric amplifier based on a GaSe nonlinear crystal and a  $\sim 2 \mu\text{m}$  pump laser. The generated idler pulse has a flat spectrum spanning from 4.5 to 13.3  $\mu\text{m}$  at -3 dB and 4.2 to 16  $\mu\text{m}$  in the full spectral range, with a central wavelength of 8.8  $\mu\text{m}$ . To our best knowledge, this is the broadest -3 dB spectrum ever obtained by optical parametric amplifiers in this spectral region. The spectrum supports  $\sim 19$  fs Fourier-transform-limited pulse width, corresponding to 0.65 cycle, centered at 8.8  $\mu\text{m}$ .  $\sim 3.4 \mu\text{J}$  pulse energy is obtained with a pump-to-idler conversion efficiency of  $\sim 2\%$ .**

**OCIS codes:** (140.3070) Infrared and far-infrared lasers; (190.4360) Nonlinear optics, devices; (190.4410) Nonlinear optics, parametric processes; (190.7110) ultrafast nonlinear optics.

<http://dx.doi.org/10.1364/OL.99.099999>

High-energy, mid-infrared (mid-IR), ultra-broadband, few-cycle lasers have been attracting extensive attentions for their applications in molecular spectroscopy [1-4] and strong-field physics [5-14]. In the recent years, the research has been extended to  $>6 \mu\text{m}$  long-wavelength mid-IR region. For molecular spectroscopic applications, the long-wavelength mid-IR is more important than the short-wavelength mid-IR, because the absorption spectrum in the wavelength range of 6.7-25  $\mu\text{m}$ , i.e. the fingerprint region, is distinctive for each molecule, which allows their unique identification [3, 4]. In the applications of strong-field physics, with long mid-IR laser wavelength, the energy of the recolliding electron increases substantially. It enables reaching deep into the tunneling ionization regime even at moderate laser intensity, without causing optical damage. The long-wavelength mid-IR few-cycle lasers have triggered a number of researches in the ultrafast electronics in molecules, solid materials as well as

nano-structures [7-14]. More interestingly, long-wavelength mid-IR pulses have their photon energies far below the typical electronic interband resonances of bulk semiconductors. So the phase-stable few-cycle long-wavelength mid-IR pulses could serve as a precisely adjustable bias for ultrafast electronics studies [11]. With the demand from the high-fidelity mid-IR spectroscopy and advanced attosecond electronics, high-energy few-cycle long-wavelength mid-IR lasers with the stable carrier-envelope (CE) phase are highly desired.

Due to the lack of broadband gain media in the mid-IR region, nonlinear down conversions such as optical parametric amplifier (OPA), optical parametric chirped-pulse amplifier (OPCPA) and difference-frequency generation (DFG) are commonly used to generate high-energy few-cycle mid-IR pulses. Non-oxide nonlinear crystals such as AgGaS<sub>2</sub> [15, 16], CdSiP<sub>2</sub> [17], and ZnGeP<sub>2</sub> [18-20] are employed to extend the high-energy few-cycle pulses to the wavelength range of 4-11  $\mu\text{m}$ . 8.5  $\mu\text{m}$ , 150  $\mu\text{J}$ , few-cycle pulses are demonstrated by mixing the 1.8  $\mu\text{m}$  pump and the 2.4  $\mu\text{m}$  signal in an AgGaS<sub>2</sub>-based DFG system [15]. 33  $\mu\text{J}$ , 0.88-cycle pulses covering 2.5-10  $\mu\text{m}$  spectral range are generated by the coherent synthesis of signal and idler pulses of a CdSiP<sub>2</sub> OPA, pumped by a 2  $\mu\text{m}$  OPCPA [17]. The energy of 7  $\mu\text{m}$ , few-cycle pulses is boosted to half milijoule in a ZnGeP<sub>2</sub>-based OPCPA system, with a powerful 2  $\mu\text{m}$  cryogenic-cooled pump [18]. Recently, the wide bandgap nonlinear crystal LiGaS<sub>2</sub> is emerging. 7-11  $\mu\text{m}$  few-cycle pulses with nano-joule-level pulse energy have been demonstrated in OPA or intrapulse DFG based on LiGaS<sub>2</sub>, pumped by near-IR pulses [21-24]. The energy scaling potential is foreseeable for this wide-bandgap crystal in the near future. In a future step, to pursue the longer wavelength up to 20  $\mu\text{m}$ , AgGaSe<sub>2</sub> [25] and GaSe [26, 27] nonlinear crystals have been employed in the DFG systems, thanks to their longer transparent wavelength cutoff. In order to achieve broad phase-matching (PM) bandwidth and avoid parasitic two- or three-photon absorption, they should ideally be pumped at  $\sim 2 \mu\text{m}$  wavelength. Compared with AgGaSe<sub>2</sub>, GaSe has higher damage threshold, larger nonlinear coefficient

( $\sim 34$  pm/V for type-II AgGaSe<sub>2</sub> and  $\sim 56$  pm/V for type-I GaSe), larger birefringence ( $\Delta n \sim 0.35$ ) and broader PM bandwidth by using  $\sim 2$   $\mu\text{m}$  pump. This makes GaSe a better candidate of generating high-energy, ultra-broadband, few-cycle, long-wavelength mid-IR pulses.

In this letter, we report a GaSe-based mid-IR OPA driven by  $\sim 2$   $\mu\text{m}$  pump for the first time. The generated ultra-broadband idler pulse from the mid-IR OPA has a central wavelength of 8.8  $\mu\text{m}$ , spanning from 4.5 to 13.3  $\mu\text{m}$  at -3 dB and 4.2 to 16  $\mu\text{m}$  in the full spectral range. To our best knowledge, this is the broadest mid-IR spectrum at -3 dB spectral range, ever obtained from the long-wavelength OPA systems. The measured spectrum supports a Fourier-transform-limited pulse width of  $\sim 19$  fs, which corresponds to 0.65 cycle, centered at 8.8  $\mu\text{m}$ .  $\sim 3.4$   $\mu\text{J}$  idler pulse energy is demonstrated with the conversion efficiency of  $\sim 2\%$ . The idler pulse has a passively stable CE phase by principle, due to the DFG nature in the OPA. We believe the generated multi-microjoule, few-cycle, ultra-broadband, long-wavelength mid-IR pulses would be impactful for both the mid-IR molecular spectroscopy and the petahertz electron dynamics studies.

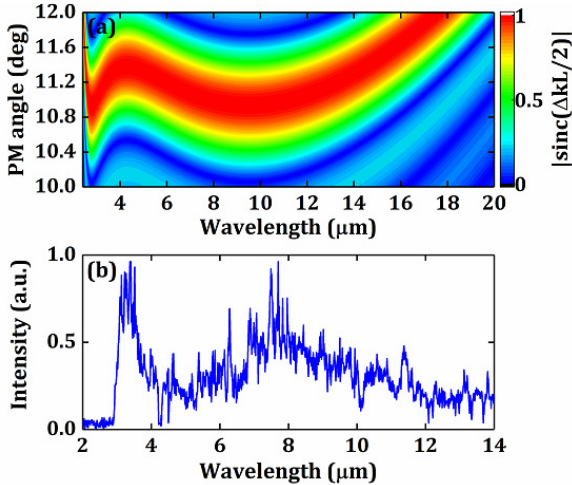


Fig. 1. (a) PM function  $|\text{sinc}(\Delta kL/2)|$  with respect to the PM angle and PM wavelength, in a GaSe crystal with a length ( $L$ ) of 1 mm, for the type-I phase match, at 2.15  $\mu\text{m}$  pump wavelength. (b) The measured optical parametric generation spectrum in a 1 mm GaSe crystal pumped by the 2.15  $\mu\text{m}$ , 51 fs laser.

GaSe has broad PM bandwidth, pumped at  $\sim 2$   $\mu\text{m}$  wavelength. Fig. 1(a) shows the PM function  $|\text{sinc}(\Delta kL/2)|$  with respect to the PM angle and the PM wavelength. Here a 1-mm thick GaSe crystal for the type-I phase match, pumped at 2.15  $\mu\text{m}$  wavelength, is used for calculation. Within 0.4 degree deviation of the PM angle, centered at  $\sim 11.1^\circ$ , the PM wavelength of the idler pulse ranging from 4 to 16  $\mu\text{m}$  could be realized. It is worth mentioning that when a broadband pump laser is used, even broader PM bandwidth is expected. The ultra-broad PM bandwidth is verified by the measured parametric generation in a 1-mm GaSe using a 2.15  $\mu\text{m}$ , 51 fs pump laser as shown in Fig. 1(b). A parametric spectrum spanning from 2.7 to  $>14$   $\mu\text{m}$  is obtained. It is to be noted that the spectral measurement of the parametric generation is

limited only in the range of 2.4-14  $\mu\text{m}$ . The spectral component of  $>14$   $\mu\text{m}$  is not measured.

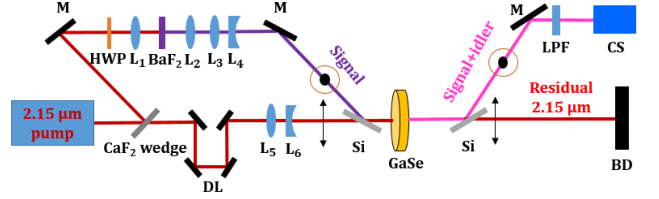


Fig. 2. The schematic of the GaSe-based mid-IR OPA. The pump, the generated supercontinuum, and the amplified mid-IR pulses are shown in maroon, purple, and pink, respectively. M, HWP, DL, LPF, and BD denotes the silver mirror, the half-wave plate, the delay line, the long-pass filter, and the beam dump, respectively. CS is the characterization setup.  $L_1$ - $L_6$  are  $\text{CaF}_2$  lenses.

The mid-IR OPA has a single amplification stage as shown in the schematic in Fig. 2. It starts with a commercial OPA system (TOPAS from Light Conversion, which is driven by a 5 mJ, 30 fs, 800 nm Ti: Sapphire laser system) with a 2.15  $\mu\text{m}$  central wavelength, 420  $\mu\text{J}$  pulse energy, 51 fs pulse width, and 1 kHz repetition rate. A  $\text{CaF}_2$  wedge placed at  $22^\circ$  with respect to the pump beam functioning as a beam splitter is employed to reflect  $\sim 10$   $\mu\text{J}$ , 2.15  $\mu\text{m}$ , p-polarized pump for the supercontinuum (SC) generation. It is rotated to s-polarization by a half-wave plate, and focused into a 6-mm thick  $\text{BaF}_2$  by  $L_1$  to generate signal pulses via SC. The generated SC is collimated by  $L_2$  and resized to  $\sim 2.5$  mm  $1/e^2$  diameter by a telescope comprised of  $L_3$  and  $L_4$ . The transmitted 2.15  $\mu\text{m}$  beam enters the pump line, which includes a delay line and a telescope ( $L_5$  and  $L_6$ ), to form a collimated pump beam with a  $1/e^2$  diameter of  $\sim 2.5$  mm. The collimated beam is then employed to pump a 1 mm-thick uncoated GaSe crystal with a type-I phase match. As the GaSe crystal could be cleaved only along the (001) plane ( $z$ -cut,  $\theta = 0^\circ$ ), an internal PM angle of  $\sim 11.1^\circ$  corresponding to an external angle of  $\sim 32^\circ$  is introduced, which causes  $\sim 16\%$  loss for the p-polarized pump. Note that the pump beam is routed to the crystal using multiple silver mirrors with  $\sim 96\%$  reflection each. Taking into account all the losses, the maximum available pulse energy of the 2.15  $\mu\text{m}$  pump is  $\sim 300$   $\mu\text{J}$ , giving an estimated peak intensity of  $\sim 224$   $\text{GW}/\text{cm}^2$ . Two 200- $\mu\text{m}$  thick silicon windows placed at Brewster angle of  $73.8^\circ$  with respect to the pump beam are used as the beam combiner and beam splitter, respectively, with  $\sim 71\%$  reflection for the s-polarized signal and idler beams. The generated idler pulse is separated from the amplified signal using a long-pass filter (LPF) with a cut-off wavelength at 4.5  $\mu\text{m}$ . It is then characterized by a thermal sensitive power meter and a mid-IR monochromator with a liquid-nitrogen-cooled MCT detector. For the spectral measurement, an uncoated ZnSe lens with a near-flat transmission over 1-15  $\mu\text{m}$  and a dielectric-coated mid-IR hollow-core fiber (from OptoKnowledge) with a near-flat transmission in the range of 3-16  $\mu\text{m}$  are employed to couple the idler pulses into the mid-IR monochromator.

The spectral and temporal profiles of the 2.15  $\mu\text{m}$  pump from TOPAS are firstly characterized. The measured spectrum as shown in Fig. 3(a) has a full width at half maximum of  $\sim 220$  nm which supports  $\sim 31$  fs Fourier-transform-limited pulse width. The intensity autocorrelation shown in Fig. 3(b) reveals the pulse width of  $\sim 51$  fs, assuming a Gaussian temporal profile. This agrees with the residual dispersion from the TOPAS optics, including

$\sim -400 \text{ fs}^2$  dispersion from the 3 mm fused silica beam splitter (reflecting 800 nm, and transmitting 2.15  $\mu\text{m}$ ). Fig. 3(c) shows the long-wavelength side of the SC spectrum (measured through a  $\text{InF}_3$  fiber and a 2.4  $\mu\text{m}$  LPF) which serves as the signal of the mid-IR OPA. It extends to  $\sim 4.3 \mu\text{m}$ . Here the influence of the nonlinear effects from the  $\text{InF}_3$  fiber on the spectral measurement has been excluded. With the knowledge of the long-wavelength edge of the signal, the calculated spectral edge on the short-wavelength side of the generated idler is  $\sim 4.3 \mu\text{m}$ , using 2.15  $\mu\text{m}$  as the pump wavelength. Thus a LPF with a 4.5  $\mu\text{m}$  cut-off wavelength is used to separate the generated idler from the amplified signal.

The spectrum of the amplified signal is shown in Fig. 3(d), measured through the mid-IR hollow-core fiber and the 2.4  $\mu\text{m}$  LPF. It is to be noticed that the short wavelength edge is limited by the mid-IR hollow-core fiber with the transmission range of 3-16  $\mu\text{m}$ , and the non-zero intensity at  $\sim 4.3 \mu\text{m}$  is attributed to the emergence of idler pulse at the degenerate wavelength.

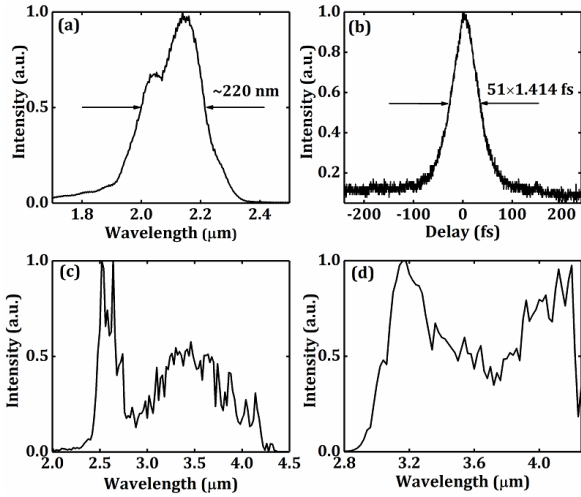


Fig. 3. (a) The measured pump spectrum from TOPAS with  $\sim 420 \mu\text{J}$  output energy. (b) The intensity autocorrelation trace of the pump pulses with  $\sim 420 \mu\text{J}$  output energy. (c) The measured spectrum of supercontinuum generation from 6-mm-thick  $\text{BaF}_2$ , which serves as the signal of the mid-IR OPA. (d) The amplified signal spectrum measured at  $\sim 300 \mu\text{J}$  pump energy.

The spectrum of the generated idler pulse is measured through the mid-IR hollow-core fiber and LPFs with different cut-off wavelengths, with 20 nm spectral resolution, as shown in Fig. 4(a). The responsivity of the MCT detector, the diffraction efficiency of the grating in the monochromator, and the transmission of LPFs, ZnSe lens and the mid-IR hollow-core fiber are calibrated over the broadband mid-IR spectral range. The possibility of the spectral shaping is carefully excluded to ensure the accuracy of the spectral measurement. The measured spectrum of the idler pulse spans from 4.2 to 16  $\mu\text{m}$ , with the -3 dB bandwidth ranging from 4.5 to 13.3  $\mu\text{m}$ . This agrees with the predicted bandwidth by the PM function shown by the maroon curve in Fig. 4(a). It should be noted that the 4.5  $\mu\text{m}$  LPF is responsible for the steep edge at  $\sim 4.6 \mu\text{m}$ . The water absorption contributes to the broad dip centered at  $\sim 5.5 \mu\text{m}$ . The peaks appearing at  $\sim 7 \mu\text{m}$  and  $\sim 12 \mu\text{m}$  are attributed to the best PM condition. It is clear that the PM function has its maximal value at these two wavelengths. The dip at  $\sim 9.6 \mu\text{m}$  is also predicted by the PM function. While the PM condition is still

satisfied over 13-15  $\mu\text{m}$ , the increasing transmission loss in GaSe beyond 13  $\mu\text{m}$  prevents the efficient idler generation, as shown in the measured spectrum.

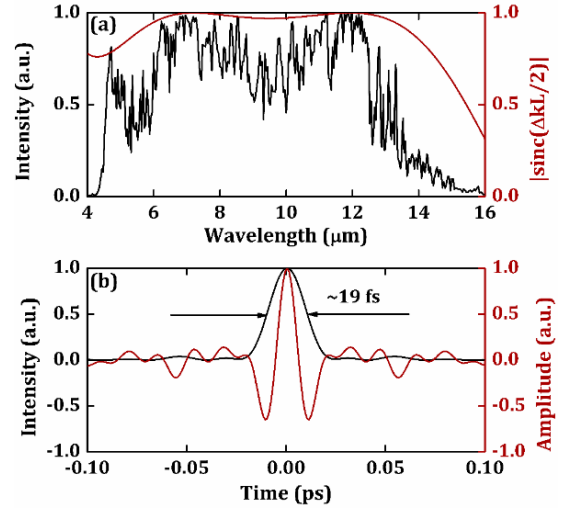


Fig. 4. (a) The measured spectrum of the generated idler pulses with  $\sim 3.4 \mu\text{J}$  output energy (black curve). The PM function  $|\text{sinc}(\Delta kL/2)|$  (maroon curve) at a PM angle of  $11.05^\circ$  is compared. The type-I phase match in the 1 mm GaSe, pumped at 2.15  $\mu\text{m}$  wavelength is used in the calculation. (b) The calculated temporal profile and electrical field of the idler pulse using the measured idler spectrum, assuming a Fourier-limited pulse, and the zero CE phase.

The temporal profile and the electric field of the generated idler pulse are calculated using the measured spectrum, assuming the idler pulse is Fourier-transform limited, and the CE phase is zero. As shown in Fig. 4(b),  $\sim 19 \text{ fs}$  transform-limited pulse width is supported, which corresponds to 0.65-cycle electric field of an 8.8  $\mu\text{m}$  center wavelength. The actual pulse width could be broadened to few cycles by the dispersion from the 1 mm thick 4.5  $\mu\text{m}$  LPF (Ge substrate) and the intrinsic dispersion from the OPA, for example, the dispersion from the 1 mm thick GaSe. Nevertheless, it could be compressed back to a near-Fourier-limited pulse using bulk materials with proper dispersions. It is worth noting that as the signal and the pump are from the same TOPAS pump system, the CE phase fluctuation in the idler pulse is self-canceled through the DFG nature of the OPA [28, 29]. Recently, the stable CE phase of the idler pulse from a passively CE phase stable mid-IR OPA has been experimentally confirmed [17]. Thus, we, to the large extent, believe that the CE phase for our system is stable. However, its CE phase stability could be degraded by some factors such as the intensity-to-phase noise of the pump, and the temporal jitters between the pump and the signal [28, 29].

The pulse energy of the generated idler is measured as  $\sim 3.4 \mu\text{J}$  behind a 4.5  $\mu\text{m}$  LPF, with  $\sim 300 \mu\text{J}$  pump energy. Considering the 85% transmission of the LPF and  $\sim 71\%$  reflection from the silicon beam splitter for idler pulses,  $\sim 2\%$  conversion efficiency from pump to idler is achieved. It is to be mentioned that for our OPA system, the measured energy of the optical parametric generation at the maximum pump energy is  $\sim 0.12 \mu\text{J}$ , and the energy fluctuation of the generated idler pulses is  $< 0.1 \mu\text{J}$ , within 30 minutes measurement time. In addition, on the long-wavelength side of the generated idler,  $\sim 1.9 \mu\text{J}$  is measured using a 7.3  $\mu\text{m}$  LPF.

The evenly distributed pulse energy in the short and long wavelength bands of the generated idler spectrum further confirms the flat spectral span as measured in Fig. 4(a). The idler pulse energies with different LPFs as a function of the pump energy are measured. As shown in Fig. 5, no saturation occurs at the maximum pump energy, which explains the obtained moderate conversion efficiency. The beam profile behind the 4.5  $\mu\text{m}$  LPF are also measured exhibiting a good Gaussian profile shown in the inset of Fig. 5. The good beam profile of the idler beam also indicates no back-conversion or crystal damage occurred. It is worth mentioning that with the rapid progress of  $\sim 2\mu\text{m}$  Ho:YLF or Ho:YAG OPCPA systems [18-20,30], the energy scaling up of the ultra-broadband mid-IR pulses is expected through the development of the GaSe-based OPCPA system.

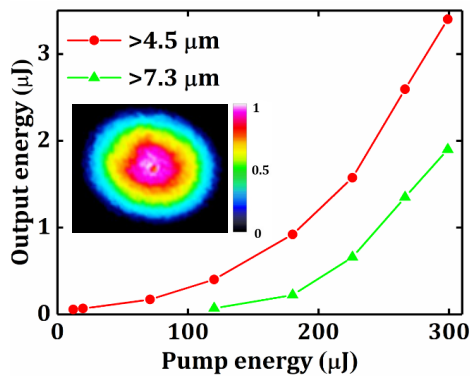


Fig. 5. The dependence of the idler pulse energy on the pump energy behind the 4.5 and 7.3  $\mu\text{m}$  LPFs. The inset is the beam profile of the idler pulse behind the 4.5  $\mu\text{m}$  LPF at the output energy of  $\sim 3.4 \mu\text{J}$ .

In conclusions, we report a GaSe-based mid-IR OPA system driven by  $\sim 2$  pump pulses, with the passively stable CE phase by principle. The idler pulse has a flat spectrum spanning from 4.5 to 13.3  $\mu\text{m}$  (at -3 dB) and 4.2 to 16  $\mu\text{m}$  (full spectrum range). To the best of our knowledge, this is the broadest -3 dB spectrum from the OPA systems at this spectral region. The measured spectrum of the idler pulse supports a pulse width of  $\sim 19$  fs, corresponding to 0.65-cycle electric field, centered at 8.8  $\mu\text{m}$ . The energy of the idler pulse is measured as  $\sim 3.4 \mu\text{J}$  with a conversion efficiency of  $\sim 2\%$ . The developed multi-microjoule, few-cycle, mid-IR laser with a broadband spectrum covering almost the entire fingerprint region is a unique source for both the mid-IR spectroscopy and strong-field electron dynamics studies.

**Acknowledgement.** We acknowledge the financial support from SERC (Grant No.1426500050, and 1426500051) from the Agency for Science, Technology and Research (A\*STAR), Singapore.

## References

1. A. Schliesser, N. Picqué, and T.W. Hänsch, *Nat. Photonics* **6**, 440 (2012).
2. J. Haas, and B. Mizaikoff, *Annu. Rev. Anal. Chem.* **9**, 45 (2016).
3. O. Kara, L. Maidment, T. Gardiner, P. G. Schunemann, and D. T. Reid, *Op. Express* **25**, 32713 (2017).
4. H. Timmers, A. Kowligy, A. Lind, F. C. Cruz, N. Nader, M. Silfies, G. Ycas, T. K. Allison, P. G. Schunemann, S. B. Papp, and S. A. Diddams, *Optica* **5**, 727 (2018).
5. J. Li, X. Ren, Y. Yin, K. Zhao, A. Chew, Y. Cheng, E. Cunningham, Y. Wang, S. Hu, Y. Wu, M. Chini and Z. Chang, *Nat. Commun.* **8**, 186 (2017).
6. T. Popmintchev, M.-C. Chen, D. Popmintchev, P. Arpin, S. Brown, S. Ališauskas, G. Andriukaitis, T. Balčiunas, O. D. Mücke, A. Pugzlys, A. Baltuška, B. Shim, S. E. Schrauth, A. Gaeta, C. Hernández-García, L. Plaja, A. Becker, A. Jaron-Becker, M. M. Murnane, and H. C. Kapteyn, *Science* **336**, 1287 (2012).
7. B. Wolter, M. G. Pullen, A-T. Le, M. Baudisch, K. Doblhoff-Dier, A. Senftleben, M. Hemmer, C. D. Schröter, J. Ullrich, T. Pfeifer, R. Moshhammer, S. Gräfe, O. Vendrell, C. D. Lin, and J. Biegert, *Science* **354**, 308 (2016).
8. L. V. Keldysh, *Sov. Phys. JETP* **20**, 1307 (1965).
9. P. Colosimo, G. Doumy, C. I. Blaga, J. Wheeler, C. Hauri, F. Catoire, J. Tate, R. Chirla, A. M. March, G. G. Paulus, H. G. Muller, P. Agostini and L.F. DiMauro, *Nat. Phys.* **4**, 386 (2008).
10. G. Herink, D. R. Solli, M. Gulde, and C. Ropers, *Nature* **483**, 190 (2012).
11. M. Hohenleutner, F. Langer, O. Schubert, M. Knorr, U. Huttner, S. W. Koch, M. Kira, and Rupert Huber, *Nature* **523**, 572 (2015).
12. S. Ghimire, A. D. DiChiara, E. Sistrunk, P. Agostini, L. F. DiMauro, and D. A. Reis, *Nat. Phys.* **7**, 138 (2011).
13. O. Schubert, M. Hohenleutner, F. Langer, B. Urbanek, C. Lange, U. Huttner, D. Golde, T. Meier, M. Kira, S. W. Koch, and R. Huber, *Nat. Photonics* **8**, 119 (2014).
14. T. Rybka, M. Ludwig, M. F. Schmalz, V. Knittel, D. Brida, and A. Leitenstorfer, *Nat. Photonics* **10**, 667 (2016).
15. G. M. Archipovaite, P. Malevich, E. Cormier, T. Lihao, A. Baltuska, and T. Balciunas, *Advanced Solid State Lasers (Optical Society of America, 2017)*, paper AM4A-4.
16. A. A. Lanin, A. A. Voronin, E. A. Stepanov, A. B. Fedotov, and A. M. Zheltikov, *Opt. Lett.* **40**, 974 (2015).
17. H. Liang, P. Krogen, Z. Wang, H. Park, T. Kroh, K. Zawilski, P. Schunemann, J. Moses, L. F. DiMauro, F. X. Kärtner, and K.-H. Hong, *Nat. Commun.* **8**, 141 (2017).
18. D. Sanchez, M. Hemmer, M. Baudisch, S. L. Cousin, K. Zawilski, P. Schunemann, O. Chalus, C. Simon-Boisson, and J. Biegert, *Optica* **3**, 147 (2016).
19. L. Grafenstein, M. Bock, D. Ueberschaer, K. Zawilski, P. Schunemann, U. Griebner, and T. Elsaesser, *Opt. Lett.* **42**, 3796 (2017).
20. T. Kanai, P. Malevich, S. S. Kangaparambil, K. Ishida, M. Mizui, K. Yamanouchi, H. Hoogland, R. Holzwarth, A. Pugzlys, and A. Baltuska, *Opt. Lett.* **42**, 683 (2017).
21. I. Pupez, D. Sánchez, J. Zhang, N. Lilienfein, M. Seidel, N. Karpowicz, T. Paasch-Colberg, I. Znakovskaya, M. Pescher, W. Schweinberger, V. Pervak, E. Fill, O. Pronin, Z. Wei, F. Krausz, A. Apolonski, and J. Biegert, *Nat. Photonics* **9**, 721 (2015).
22. B.-H. Chen, T. Nagy, and P. Baum, *Opt. Lett.* **43**, 1742 (2018).
23. M. Seidel, X. Xiao, S. A. Hussain, G. Arisholm, A. Hartung, K. T. Zawilski, P. G. Schunemann, F. Habel, M. Trubetskov, V. Pervak, O. Pronin, and F. Krausz, *Sci. Adv.* **4**, eaaq 1526 (2018).
24. S.B. Penwell, L. Whaley-Mayda, and A. Tokmakoff, *Opt. Lett.* **43**, 1363 (2018).
25. O. Novák, P. R. Krogen, T. Kroh, T. Mocek, F. X. Kärtner, and K.-H. Hong, *Opt. Lett.* **43**, 1335 (2018).
26. M. Knorr, J. Raab, M. Tauer, P. Merkl, D. Peller, E. Wittmann, E. Riedle, C. Lange, and R. Huber, *Opt. Lett.* **42**, 4367 (2017).
27. J. Zhang, K. F. Mak, N. Nagl, M. Seidel, D. Bauer, D. Sutter, V. Pervak, F. Krausz, and O. Pronin, *Light Sci. Appl.* **7**, 17180 (2018).
28. A. Baltuška, T. Fuji, and T. Kobayashi, *Phys. Rev. Lett.* **88**, 133901 (2002).
29. G. Cerullo, A. Baltuška, O. Mücke, and C. Vozzi, *Laser Photonics Rev.* **5**, 323 (2011).
30. L. von Grafenstein, M. Bock, D. Ueberschaer, U. Griebner, and T. Elsaesser, *Opt. Lett.* **41**, 4668 (2016).

## Full references

1. A. Schliesser, N. Picqué, and T.W. Hänsch, "Mid-infrared frequency combs," *Nat. Photonics* **6**, 440 (2012).
2. J. Haas, and B. Mizaikoff, "Advances in mid-infrared spectroscopy for chemical analysis," *Annu. Rev. Anal. Chem.* **9**, 45 (2016).
3. O. Kara, L. Maidment, T. Gardiner, P. G. Schunemann, and D. T. Reid, "Dual-comb spectroscopy in the spectral fingerprint region using OPGaP optical parametric oscillators," *Op. Express* **25**, 32713 (2017).
4. H. Timmers, A. Kowligy, A. Lind, F. C. Cruz, N. Nader, M. Silfies, G. Ycas, T. K. Allison, P. G. Schunemann, S. B. Papp, and S. A. Diddams, "Molecular fingerprinting with bright, broadband infrared frequency combs," *Optica* **5**, 727 (2018).
5. J. Li, X. Ren, Y. Yin, K. Zhao, A. Chew, Y. Cheng, E. Cunningham, Y. Wang, S. Hu, Y. Wu, M. Chini and Z. Chang, "53-attosecond X-ray pulses reach the carbon K-edge," *Nat. Commun.* **8**, 186 (2017).
6. T. Popmintchev, M.-C. Chen, D. Popmintchev, P. Arpin, S. Brown, S. Ališauskas, G. Andriukaitis, T. Balčiunas, O. D. Mücke, A. Pugzlys, A. Baltuška, B. Shim, S. E. Schrauth, A. Gaeta, C. Hernández-García, L. Plaja, A. Becker, A. Jaron-Becker, M. M. Murnane, and H. C. Kapteyn, "Bright coherent ultrahigh harmonics in the keV x-ray regime from midinfrared femtosecond lasers," *Science* **336**, 1287 (2012).
7. B. Wolter, M. G. Pullen, A.-T. Le, M. Baudisch, K. Doblhoff-Dier, A. Senfleben, M. Hemmer, C. D. Schröter, J. Ullrich, T. Pfeifer, R. Moshhammer, S. Gräfe, O. Vendrell, C. D. Lin, and J. Biegert, "Ultrafast electron diffraction imaging of bond breaking in di-ionized acetylene," *Science* **354**, 308 (2016).
8. L. V. Keldysh, "Ionization in the field of a strong electromagnetic wave," *Sov. Phys. JETP* **20**, 1307 (1965).
9. P. Colosimo, G. Doumy, C. I. Blaga, J. Wheeler, C. Hauri, F. Catoire, J. Tate, R. Chirla, A. M. March, G. G. Paulus, H. G. Muller, P. Agostini and L.F. DiMauro, "Scaling strong-field interactions towards the classical limit," *Nat. Phys.* **4**, 386 (2008).
10. G. Herink, D. R. Solli, M. Gulde, and C. Ropers, "Field-driven photoemission from nanostructures quenches the quiver motion," *Nature* **483**, 190 (2012).
11. M. Hohenleutner, F. Langer, O. Schubert, M. Knorr, U. Huttner, S. W. Koch, M. Kira, and Rupert Huber, "Real-time observation of interfering crystal electrons in high-harmonic generation," *Nature* **523**, 572 (2015).
12. S. Ghimire, A. D. DiChiara, E. Sistrunk, P. Agostini, L. F. DiMauro, and D. A. Reis, "Observation of high-order harmonic generation in a bulk crystal," *Nat. Phys.* **7**, 138 (2011).
13. O. Schubert, M. Hohenleutner, F. Langer, B. Urbanek, C. Lange, U. Huttner, D. Golde, T. Meier, M. Kira, S. W. Koch, and R. Huber, "Sub-cycle control of terahertz high-harmonic generation by dynamical Bloch oscillations," *Nat. Photonics* **8**, 119 (2014).
14. T. Rybka, M. Ludwig, M. F. Schmalz, V. Knittel, D. Brida, and A. Leitenstorfer, "Sub-cycle optical phase control of nanotunnelling in the single-electron regime," *Nat. Photonics* **10**, 667 (2016).
15. G. M. Archipovaite, P. Malevich, E. Cormier, T. Lihao, A. Baltuska, and T. Balciunas, "Efficient few-cycle mid-IR pulse generation in the 5-11  $\mu\text{m}$  window driven by an Yb amplifier," *Advanced Solid State Lasers (Optical Society of America, 2017)*, paper AM4A-4.
16. A. A. Lanin, A. A. Voronin, E. A. Stepanov, A. B. Fedotov, and A. M. Zheltikov, "Multioctave, 3–18  $\mu\text{m}$  sub-two-cycle supercontinua from self-compressing, self-focusing soliton transients in a solid," *Opt. Lett.* **40**, 974 (2015).
17. H. Liang, P. Krogen, Z. Wang, H. Park, T. Kroh, K. Zawilski, P. Schunemann, J. Moses, L. F. DiMauro, F. X. Kärtner, and K.-H. Hong, "High-energy mid-infrared sub-cycle pulse synthesis from a parametric amplifier," *Nat. Commun.* **8**, 141 (2017).
18. D. Sanchez, M. Hemmer, M. Baudisch, S. L. Cousin, K. Zawilski, P. Schunemann, O. Chalus, C. Simon-Boisson, and J. Biegert, "7  $\mu\text{m}$ , ultrafast, sub-millijoule-level mid-infrared optical parametric chirped pulse amplifier pumped at 2  $\mu\text{m}$ ," *Optica* **3**, 147 (2016).
19. L. Grafenstein, M. Bock, D. Ueberschaer, K. Zawilski, P. Schunemann, U. Griebner, and T. Elsaesser, "5  $\mu\text{m}$  few-cycle pulses with multi-gigawatt peak power at a 1 kHz repetition rate," *Opt. Lett.* **42**, 3796 (2017).
20. T. Kanai, P. Malevich, S. S. Kangaparambil, K. Ishida, M. Mizui, K. Yamanouchi, H. Hoogland, R. Holzwarth, A. Pugzlys, and A. Baltuska, "Parametric amplification of 100 fs mid-infrared pulses in ZnGeP2 driven by a Ho:YAG chirped-pulse amplifier," *Opt. Lett.* **42**, 683(2017).
21. I. Pupeza, D. Sánchez, J. Zhang, N. Lilienfein, M. Seidel, N. Karpowicz, T. Paasch-Colberg, I. Znakovskaya, M. Pescher, W. Schweinberger, V. Pervak, E. Fill, O. Pronin, Z. Wei, F. Krausz, A. Apolonski, and J. Biegert, "High-power sub-two-cycle mid-infrared pulses at 100 MHz repetition rate," *Nat. Photonics* **9**, 721 (2015).
22. B.-H. Chen, T. Nagy, and P. Baum, "Efficient middle-infrared generation in LiGaS2 by simultaneous spectral broadening and difference-frequency generation," *Opt. Lett.* **43**, 1742 (2018).
23. M. Seidel, X. Xiao, S. A. Hussain, G. Arisholm, A. Hartung, K. T. Zawilski, P. G. Schunemann, F. Habel, M. Trubetskov, V. Pervak, O. Pronin, and F. Krausz, "Multi-watt, multi-octave, mid-infrared femtosecond source," *Sci. Adv.* **4**, eaaq 1526 (2018).
24. S.B. Penwell, L. Whaley-Mayda, and A. Tokmakoff, "Single-stage MHz mid-IR OPA using LiGaS 2 and a fiber laser pump source," *Opt. Lett.* **43**, 1363 (2018).
25. O. Novák, P. R. Krogen, T. Kroh, T. Mocek, F. X. Kärtner, and K.-H. Hong, "Femtosecond 8.5  $\mu\text{m}$  source based on intrapulse difference-frequency generation of 2.1  $\mu\text{m}$  pulses," *Opt. Lett.* **43**, 1335 (2018).
26. M. Knorr, J. Raab, M. Tauer, P. Merkl, D. Peller, E. Wittmann, E. Riedle, C. Lange, and R. Huber, "Phase-locked multi-terahertz electric fields exceeding 13 MV/cm at a 190 kHz repetition rate," *Opt. Lett.* **42**, 4367 (2017).
27. J. Zhang, K. F. Mak, N. Nagl, M. Seidel, D. Bauer, D. Sutter, V. Pervak, F. Krausz, and O. Pronin, "Multi-mW, few-cycle mid-infrared continuum spanning from 500 to 2250  $\text{cm}^{-1}$ ," *Light Sci. Appl.* **7**, 17180 (2018).
28. A. Baltuška, T. Fuji, and T. Kobayashi, "Controlling the Carrier-Envelope Phase of Ultrashort Light Pulses with Optical Parametric Amplifiers," *Phys. Rev. Lett.* **88**, 133901 (2002).
29. G. Cerullo, A. Baltuška, O. Mücke, and C. Vozzi, "Few-optical-cycle light pulses with passive carrier-envelope phase stabilization," *Laser Photonics Rev.* **5**, 323 (2011).
30. L. von Grafenstein, M. Bock, D. Ueberschaer, U. Griebner, and T. Elsaesser, "Ho:YLF chirped pulse amplification at kilohertz repetition rates – 4.3 ps pulses at 2  $\mu\text{m}$  with GW peak power," *Opt. Lett.* **41**, 4668 (2016).